Nuclear Instruments and Methods in Physics Research A 786 (2015) 113–119

Contents lists available at ScienceDirect

Nuclear Instruments and Methods in Physics Research A

journal homepage: www.elsevier.com/locate/nima

Monte Carlo application based on GEANT4 toolkit to simulate a laser–plasma electron beam line for radiobiological studies

D. Lamia [a], G. Russo [a,*], C. Casarino [a], L. Gagliano [a], G. C. Candiano [a], L. Labate [b,e], F. Baffigi [b], L. Fulgentini [b], A. Giulietti [b], P. Koester [b], D. Palla [b], L. A. Gizzi [b,e], M. C. Gilardi [c,d]

[a] Institute of Molecular Bioimaging and Physiology IBFM CNR – LATO, Cefalù, Italy
[b] Intense Laser Irradiation Laboratory (ILIL) – National Institute of Optics INO CNR, Pisa, Italy
[c] Institute of Molecular Bioimaging and Physiology IBFM CNR, Segrate, Italy
[d] University of Milano-Bicocca, Milano, Italy
[e] National Institute for Nuclear Physics INFN, Pisa Section and Frascati National Laboratories LNF, Italy

ARTICLE INFO

Article history:
Received 12 December 2014
Received in revised form
19 February 2015
Accepted 16 March 2015
Available online 25 March 2015

Keywords:
GEANT4
Laser-driven beams
IOERT
Medical applications

ABSTRACT

We report on the development of a Monte Carlo application, based on the GEANT4 toolkit, for the characterization and optimization of electron beams for clinical applications produced by a laser-driven plasma source. The GEANT4 application is conceived so as to represent in the most general way the physical and geometrical features of a typical laser-driven accelerator. It is designed to provide standard dosimetric figures such as percentage dose depth curves, two-dimensional dose distributions and 3D dose profiles at different positions both inside and outside the interaction chamber. The application was validated by comparing its predictions to experimental measurements carried out on a real laser-driven accelerator. The work is aimed at optimizing the source, by using this novel application, for radiobiological studies and, in perspective, for medical applications.

1. Introduction

The technique of accelerating particles by means of high intensity lasers is of considerable interest in many fields of research and this technique seems to be particularly adaptable for medical applications [1,2].

Electron accelerators based on the Laser WakeField Acceleration (LWFA) mechanism in a plasma (see Ref. [3]) are attracting growing attention, mainly due to their intrinsic reduced footprint when compared to conventional LINACs. This feature is of particular importance in view of possible applications in medicine, and in particular for radiotherapy.

As is well known, the LWFA process basically relies on the excitation, due to the ponderomotive force, of a plasma wave in the wake of an ultrashort and ultraintense laser pulse propagating in an underdense plasma. Such a plasma wave exhibits the correct features to sustain the acceleration of electrons up to relativistic energies, such as a very intense longitudinal electric field (many orders of magnitude higher than in a typical radio frequency (RF) cavity LINAC) and a phase velocity close to the speed of light.

Over the past few years, laser-driven electron accelerators have evolved greatly, in terms of operation stability and reliability, so that their possible use for radiotherapy, such as, for instance, Intra-Operative Electron Radiation Therapy (IOERT), can be foreseen within the next decade. Indeed, the stable production of electron bunches with energies up to tens or even hundreds of MeV have been demonstrated to be easily achievable, thus representing a new option for radiotherapy applications. From a practical point of view, laser-driven electron accelerators would exhibit a wealth of advantages over conventional ones in terms of radioprotection requirements and flexibility. The use of a laser-driven accelerator for IOERT would allow a much smaller device to be introduced into the operating room, as the most bulky component, the laser system, may be placed and monitored outside, leaving only the "accelerator stage", a few centimeters in size, close to the patient.

A laser-driven electron accelerator features an electron bunch duration much smaller than a conventional accelerator [4]. In fact, while durations of a few up to a few tens of femtoseconds have been reported for the bunches on leaving the plasma, a bunch duration of a few picoseconds can be safely estimated/calculated at the position of the biological sample or patient (that is, after a few tens of centimeters propagation and possibly a vacuum–air interface); this value is still about six orders of magnitude higher than that of a typical LINAC used in radiotherapy. By taking into account the typical bunch charge in the two cases (which is more or less comparable), one can easily realize that a much higher

* Corresponding author.
E-mail addresses: debora.lamia@ibfm.cnr.it (D. Lamia), giorgio.russo@ibfm.cnr.it (G. Russo).

http://dx.doi.org/10.1016/j.nima.2015.03.044
0168-9002/

instantaneous dose rate is actually obtained, whose biological consequences have still to be investigated in depth. Further differences of a laser-driven accelerator when compared to a conventional one rely on the broader energy spectrum (when no advanced injection schemes are implemented, such as in the typical case of a tentatively "easy-to-use" accelerator for medicine) and a higher divergence. Before carrying out radiobiological measurements and consequently preclinical experiments, a beam characterization has to be established. To date the radiobiological effectiveness of these very intense pulses is not known with precision, thus it is important to get a suitable acceleration system to conduct these biological research activities [5]. All of these characteristics of a laser-driven accelerator require accurate studies related to dosimetric and biological issues.

In this paper we present a study directed at validating a Monte Carlo simulation tool, based on the GEANT4 toolkit, developed especially for a laser-driven accelerator. The validation was performed by comparing numerical simulations with real measurements carried out utilizing the laser-driven accelerator installed at Istituto Nazionale di Ottica (INO). Depth–dose measurements were effected inside the vacuum chamber and in the sample position using gafchromic film detectors (Fig. 1). Two-dimensional dose distributions, 3D dose profiles and PDD (Percentage Depth Dose) curves were obtained. The two-dimensional dose distributions and 3D dose profiles show the homogeneity and symmetry of the incident beam. PDD curves show the percentage of absorbed dose deposited by the radiation beam in the medium to various depths along the axis of the beam.

Monte Carlo simulations have been the main instrument to validate the dosimetric characterization of the beam, using the GEANT4 tool [6]. GEANT4 is a toolkit for the simulation of the interaction of radiation with matter which take into account all the physical processes that involve the single particle that passes through the medium. In the GEANT4 application the geometry of the acceleration system reproducing the sizes, the shapes of the experimental set-up and the materials is reconstructed. From GEANT4 simulations, the energy distribution and angular spread of the beam can be evaluated. Moreover, two-dimensional distributions and 3D profiles of dose and PDD curves were obtained . These were compared with those obtained experimentally by gafchromic films [7]. The two data sets are comparable with a specific energy distribution and a precise angular spread of the beam. At first these parameters were obtained in the configuration within the vacuum chamber. The same parameters were set in the configuration sample position in the air to verify that the parameters were actually those. The validated GEANT4 application could be used to simulate future radiobiological measurements and provide the appropriate data about the experimental set-up to carry out biological experiments in the best way.

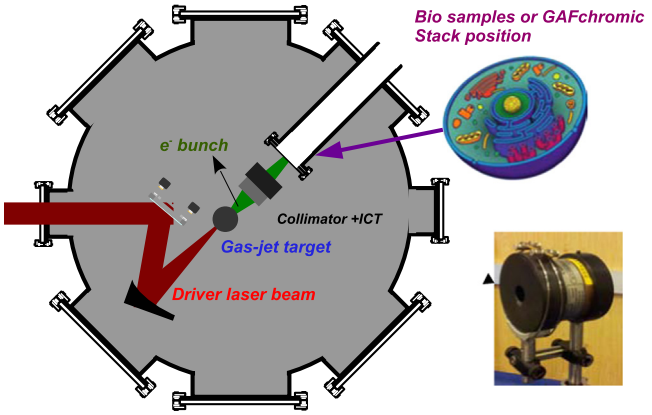

Fig. 1. Schematic layout of the experimental set-up used for the experimental validation.

2. The *laser_IOERT* application general design

In this section we describe the general features of the application we have developed, which we called *laser_IOERT*. For the sake of a clearer discussion, we bring forward the description of the experimental setup used for the experimental validation, in order to give a general idea of a typical laser-driven accelerator.

2.1. The laser–plasma based accelerator

The experimental validation reported below was carried out at the Intense Laser Irradiation Laboratory of the INO of the CNR in Pisa, where a laser-driven accelerator based upon a 10 TW Ti:Sa laser system is operating [5,8]. The laser delivers up to 450 mJ on target and features an M^2 quality factor close to 1.5 and a nanosecond contrast of about 10^{10}. For the experiments reported here, the laser was focused using an $f/4.5$ Off-Axis Parabola down to a spot size of around 10 μm FWHM; the intensity on target was of about 8×10^{18} W/cm^2. The target was made up of a supersonic nitrogen (N_2) gas-jet, produced using a rectangular nozzle with a size of 4×1.2 mm^2 (the laser propagation occurring along the smallest size); the backing pressure was kept at 50 bar. A schematic layout of the set-up inside the interaction chamber is provided in Fig. 1. The laser–plasma interaction was monitored mainly using shadowgraphy and a Thomson imaging diagnostic system (not shown in the figure). The electron production was sought and monitored using a LANEX scintillator screen imaged out by a commercial reflex camera and NaI scintillators coupled to photomultipliers (not shown in the figure). The electron spectrum was measured on a daily basis, at the beginning of each run, using a magnetic spectrometer, featuring a 1 T magnetic field and 0.5 in. length; its configuration allowed electrons with an energy greater than 4 MeV to be detected.

As shown in Fig. 1, a tube was inserted into the chamber flange along the electron propagation direction, ending with a vacuum–air interface for the electron beam made up of a 50 μm kapton layer. The electron beam production and total charge was measured on each shot using an Integrating Current Transformer (ICT) device, shown in the inset of Fig. 1. Finally, in order to prevent unwanted high-energy electrons to spread around in the vacuum chamber, a sort of collimator was created (shown in Fig. 1), made up of a sandwich structure of different plastic and metallic layers with an overall length of around 2 cm. The experimental measurements carried out for this work do not use a collimation system, so as to study the energy distribution of the beam and the angular spread.

2.2. The laser_IOERT structure: GEANT4 set-up

GEANT4 is an object-oriented toolkit developed to simulate the passage of particles through matter. It contains a large variety of physics models covering the interaction of electrons, muons, hadrons and ions with matter from 250 eV up to several PeV. Thanks to these features and due to its versatility, GEANT4 applications are developed not only in particle physics but also in many other fields where high accuracy and precision of simulations are needed, such as radiation physics, space science and medical physics. The simulation set-up is derived from a GEANT4 advanced example, *iort_therapy* [9].

Iort_therapy is published in GEANT4.9.5 version; the example is implemented to address typical needs related to the IOERT technique. Such needs can include the calculation of dose

distribution curves in water or other materials, the possibility of choosing among different clinical set-up, and the study of radio-protection devices.

Different implementations of physics processes are used, providing equivalent or alternative modeling approaches. Indeed, for electrons, positrons, and photons, different physics lists are available [10], the main differences are the physical models used and, consequently, the covered energetic range. For the *laser_IOERT* application we selected the *LowEm_Penelope* physics models. *LowEm_Penelope* is the Geant4 implementation of the physics models developed for the PENELOPE (PENetration and Energy LOss of Positrons and Electrons) code [11]. The Penelope models have been specifically developed for Monte Carlo simulation and great care was given to the low energy description. Hence, these implementations provide reliable results for energies in the range 1 keV – 10 GeV. The *LowEm_Penelope* take into account the following interactions: Compton scattering, photoelectric effect, Rayleigh scattering, gamma conversion, bremsstrahlung, ionization and positron annihilation.

Starting from *iort_therapy* the geometry of the experimental set-up was implemented [12]. The application simulates the electron beam starting from the gas-jet structure to the stack position where the irradiated samples are located. The simulated geometric components are the following: gas-jet, kapton window, two flanges and cylinder that contains the samples; everything is located in the interaction chamber (Fig. 2). In the real experimental set-up, the electron beam is generated from the interaction between the laser and gas, in the simulations one considers the electron beam already generated. Indeed Geant4 is well suited for the development of computational tools for analysing interactions of particle with matter. By the use of this toolkit it is not possible to obtain information about the laser-driven acceleration technique which can be simulated by using Particle-In-Cell codes [13].

In order to account for the possible spreading and/or slowing down effects due to the propagation in the residual neutral gas that the bunch has to cross after its acceleration in the plasma, a thin layer of gas is inserted just after the electron source. In the case considered here, 800 μm of nitrogen are considered, with a density of 0.05826 g/cm^3.

In order to cope with the large energy spread typical of the laser-driven acceleration, the GEANT4 application that simulates the LDA system allows the choice of two kinds of energy distributions: a polynomial distribution and a Gaussian/exponential mixture. The polynomial distribution was implemented in the GEANT4 application to give the opportunity to the user to study the electron beams with unusual energy spectra. In particular the polynomial distribution is 8-th degree polynomial, while the mixture is of the following form:

$$p(E) = \omega \cdot \frac{1}{\sqrt{2\pi}\sigma} e^{-(E-\mu)^2/2\sigma^2} + (1-\omega) \cdot \lambda e^{-E/\lambda} u(E) \quad (1)$$

where $0 \le \omega \le 1$. It should be noted that it can obtain a pure exponential or a pure Gaussian distribution by posing, respectively, $\omega = 0$ and $\omega = 1$. To simulate the laser-driven system the exponential energy distribution is selected.

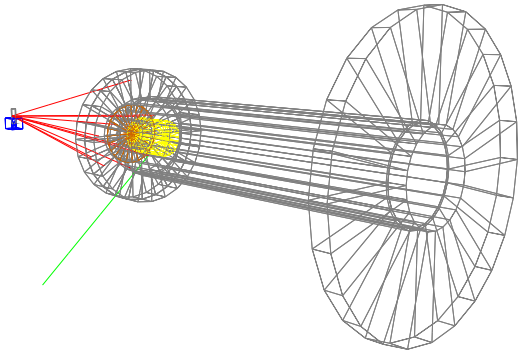

Fig. 2. GEANT4 graphic visualization of the laser-driven acceleration system. The electron beam generated from the gas-jet structure and the photons emitted by bremsstrahlung radiation are represented by lines with different colours. The largest structure contains the sample, represented by a small cylinder. (For interpretation of the references to color in this figure caption, the reader is referred to the web version of this article.)

3. Experimental validation: optimization and dosimetric characterization of a laser-driven accelerator for radiobiology experiments

In what follows we report on the use of our *laser_IOERT* application for the optimization and study of a laser-driven accelerator set-up for radiobiology experiments. The aim of this experimental work was two-fold: (a) validating the results from our code against real experimental data and (b) optimize and characterize, from the dosimetric point of view, the setup for irradiation of biological tissues.

Preliminarily, we start providing a brief report on the dosimetric characterization of the EBT3 gafchromic films used for the dosimetric measurements. Then we proceed with the dosimetric characterization of the laser-driven acceleration system with the description of experimental setup, data analysis and results obtained.

3.1. Dosimetric characterization of the EBT gafchromic films

The EBT3 gafchromic model was constructed by combining the layers of polyester with active radiosensitive layers. The active layer of 27 μm was located between two substrates made of 100 μm polyester to protect the film from external agents. The radiation led to a polymerization of the compound that constitutes the active layer, giving rise to a darkening of the film that is proportional to the absorbed radiation [14].

The EBT3 films were calibrated with a commercial LINAC Novac7 (NRT, Aprilia, Italy [15]), RF LINAC accelerator used for IOERT treatments. They were irradiated at various dose values, from 0.4 Gy to 10 Gy to obtain a calibration curve.

An Epson Expression 10000XL scanner and its associated software, EPSON SCAN v3.04, were used to read all films. Images were acquired in transmit mode and in landscape orientation where the short side of the film is oriented parallel to the scan direction, as recommended by the manufacturer [16]. The films were positioned in the center of the scanner in the direction perpendicular to the scan direction.

Images were collected at a depth of 16 bits per color channel (red, green, blue) with a spatial resolution of 72 dpi corresponding to a pixel size of 0.35 × 0.35 mm^2, and saved in tiff format.

The red channel had a greater response up to 10 Gy, the green channel exceeded the red one for doses above 10 Gy, indicating it could be preferable to use the green channel at higher doses. The blue channel had a lower response gradient at all doses, so it is less useful than the other channels for dose measurements. The digital images were then analyzed with Matlab software.

For the purpose of this work was not necessary to use the green channel, so a curve fitting was obtained only in the red channel. Fig. 3 shows the dose values as a function of the pixel values that were obtained by the scan of gafchromic films. The best agreement was set up with a polynomial curve fitting of the fourth degree.

From the calibration curve dose values corresponding to gafchromic films irradiated by the laser–plasma accelerator were obtained. These films have a high temporal resolution, are energy independent and are also dose value per pulse independent [17].

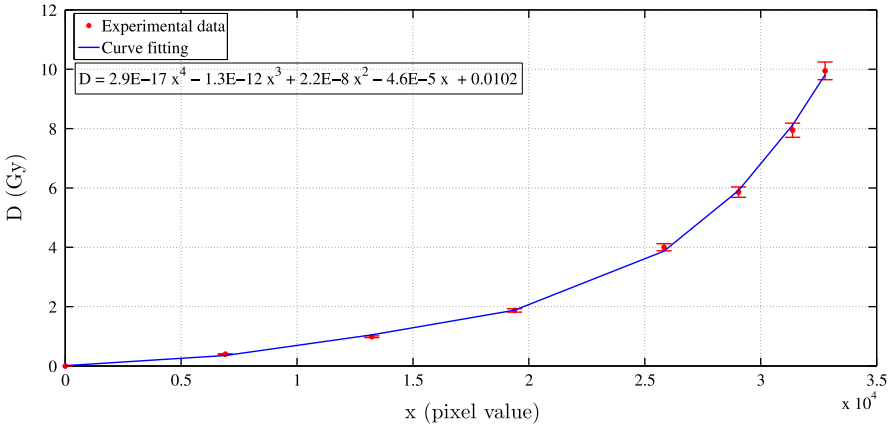

Fig. 3. EBT3 films calibration curve in the red channel (up to 10 Gy). The points represent the dose values as a function of the pixel values obtained from gafchromic films analysis. The curve is the best fitting curve obtained. (For interpretation of the references to color in this figure caption, the reader is referred to the web version of this article.)

Therefore using gafchromic films a complete dosimetric characterization of the particle beam can be obtained.

3.2. Dosimetric characterization of the laser-driven acceleration system: measurements and data analysis

Two types of experimental measurements were carried out: inside the vacuum chamber and within the sample position.

Sheets of water-equivalent RW3 material (PTW [18]) were placed inside the vacuum chamber. These sheets were $30 \times 30\ \mathrm{cm}^2$ with variable thickness: 1 mm, 2 mm, 5 mm and 10 mm. Eight sheets were placed for a total thickness of RW3 of 5 cm. Between the sheets, EBT3 gafchromic films were placed, centered in the perpendicular direction of the incident electron beam. The distance between the beam source and the first sheet of RW3 was 9.5 cm. 100 laser pulses with a frequency 0.5 Hz were issued.

Sheets of plexiglass were positioned outside the vacuum chamber, in the sample position. They were circular with a diameter of 26.5 mm and with variable thickness: 1 mm, 2 mm, 5 mm and 10 mm. In total six sheets were placed for a total thickness of plexiglass of 3 cm. EBT3 gafchromic films were placed between the sheets. The distance between the beam source and the first plexiglass sheet was 20.3 cm. 150 laser pulses were issued with a frequency 0.5 Hz.

Experimental measurements were focused on performing a characterization of the electron beam. The PDD curves, two-dimensional dose distributions and 3D dose profiles were studied. All of these observational results were compared with the ones obtained by GEANT4 simulations. To verify that simulated and experimental PDD curves are comparable a vacuum validation test was performed.

The problem considering the curves that interpolate the data was also addressed. They are continuous curves so it was not possible to use a classical statistical test, such as the Kolmogorov or Anderson test [19]. A metric test that takes into account the spatial difference between the two curves was performed. It considered $d_{\%,m}(x)$ the measured dose along the x-axis and $d_{\%,c}(x)$ the calculated dose from simulations along the same axis, varying the x coordinates. The percentage error was computed as

$$e_{\%}(x) = \left|1 - \frac{D_{\%,m}(x)}{D_{\%,c}(x)}\right| \tag{2}$$

where

$$D_{\%,m}(x) = \frac{\int_{x_{min}}^{x} d_{\%,m}(x)\,dx}{\int_{x_{min}}^{x_{max}} d_{\%,m}(x)\,dx} \tag{3}$$

$$D_{\%,c}(x) = \frac{\int_{x_{min}}^{x} d_{\%,c}(x)\,dx}{\int_{x_{min}}^{x_{max}} d_{\%,c}(x)\,dx} \tag{4}$$

Eq. (2) gives the error by varying the x coordinate, an upper limit to this can be obtained by getting

$$e_{\%} = \sup_{x} e_{\%}(x). \tag{5}$$

A value of $e_{\%}$ equal to zero implies the two distribution are the same.

The GEANT4 validated application, obtained from the simulated data, was used to study the two-dimensional dose distribution and 3D dose profiles in the sample position; they were compared with the experimental ones, measured using the gafchromic films.

Two-dimensional dose distributions with respect to the two axes perpendicular to the direction of propagation of the beam were compared: with the vertical axis as the y-axis and the horizontal axis as the z-axis.

To describe the behaviour of the lateral dose depth obtained from the simulation $d_{profile}$, a B-Spline function representation was adopted:

$$\phi^p(x) = \sum_{j=0}^{n} \alpha_j \phi_j^p(x) \tag{6}$$

where each ϕ_j^p is defined in a recursive manner as follows:

$$\phi_j^0(x) = \begin{cases} 1 & x \in [x_j, x_{j+1}) \\ 0 & \text{otherwise} \end{cases} \tag{7}$$

for each $j = 0, \ldots, m$, while for $p \geq 1$ the formulation is given as follows:

$$\phi_j^p(x) = \frac{x - x_i}{x_{i+p} - x_i}\phi_j^{p-1}(x) + \frac{x_{i+p+1} - x}{x_{i+p+1} - x_{i+1}}\phi_{j+1}^{p-1}(x). \tag{8}$$

In Eq. (6), for fixed p and n, the α_j coefficients are obtained as the solution of the problem

$$e(\alpha_1, \ldots, \alpha_n) = \left\|\phi^p - d_{profile}\right\|^2 \tag{9}$$

a complete description of both B-Spline functions and the solution of the LSE problem could be found in Ref. [20].

3.3. Dosimetric characterization of the laser-driven acceleration system: results

The depth–dose curves for both the measurement made in the vacuum chamber and for that performed within the sample position were obtained. In the case of the measurement performed with plexiglass sheets, the depth values were converted into the

corresponding depth values in water [21]. An error of 3% to the dose values measured was assigned [22].

Using iterative simulations, the energy distribution and the spread angle for which the experimental and simulated PDD curves are comparable were obtained. The energy distribution of the electron bunches at the source is assumed to be represented by an exponential distribution. The best match between simulated and experimental PDD curves is achieved with an exponential energy distribution with mean energy 1.5 MeV and with an angular gaussian distribution with FWHM of 26° spread angle. These results are validated in the sample position configuration by the PDD curve that is shown in Fig. 4 and by two-dimensional dose distributions and 3D dose profile shown in Figs. 5 and 6, respectively. For comparison profiles obtained at a depth of 2 mm were selected, where the first gafchromic film between the plexiglass sheets in the sample position was positioned.

Fig. 4 shows the percentage dose values as a function of the depth. The dose values were obtained as peak dose for every gafchromic film, that is to say the mean dose obtained in the uniform irradiated area.

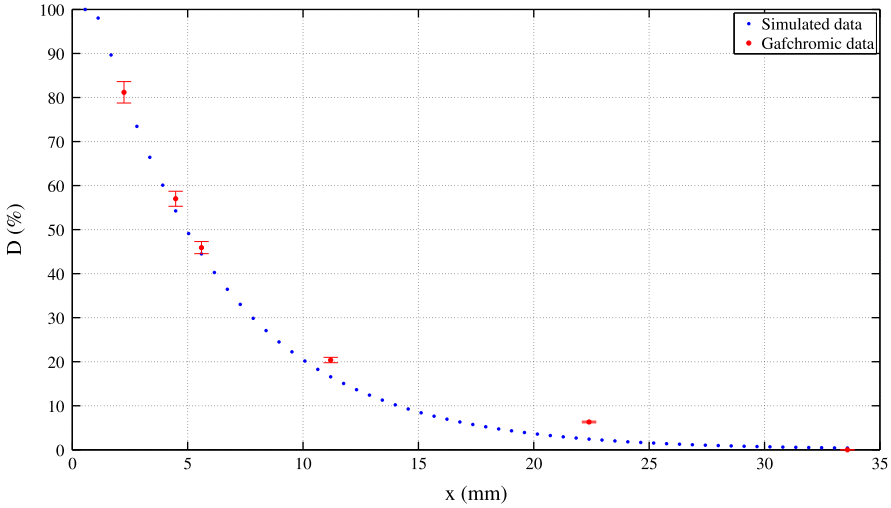

Fig. 4. Percentage dose depth curve. Comparison between experimental and simulated data.

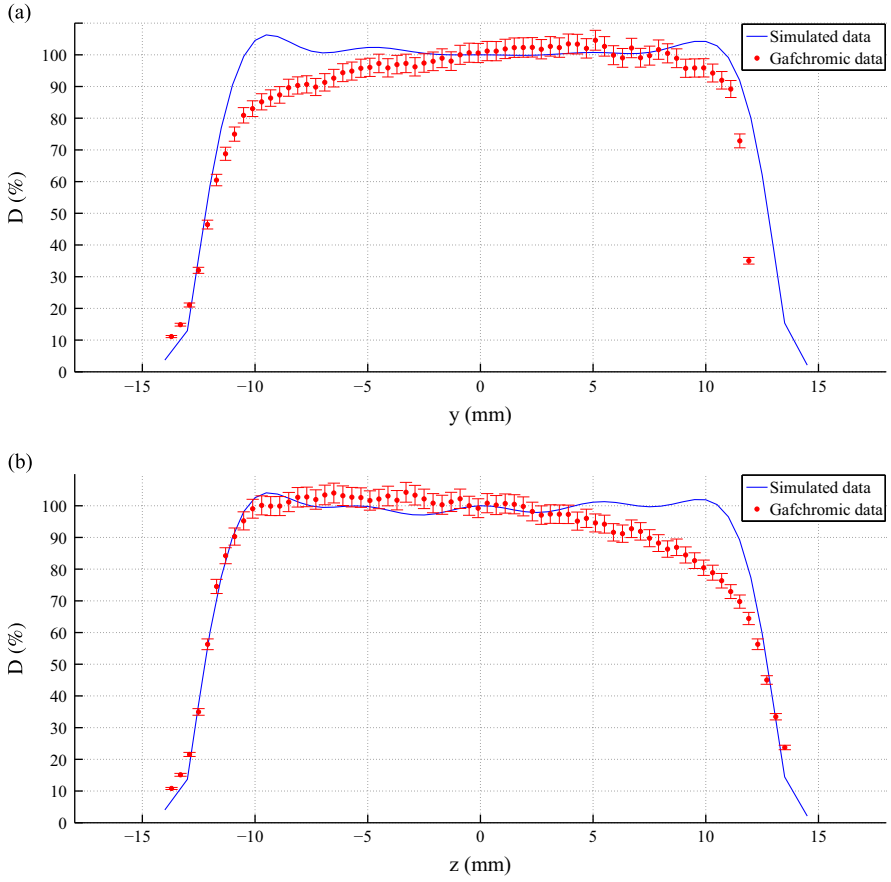

Fig. 5. Two-dimensional dose distribution along the vertical axis *y* (a) and along the horizontal axis *z* (b). The curves represent the simulated data fitted by B-spline curves. The points are the experimental data obtained from the EBT3 film analysis.

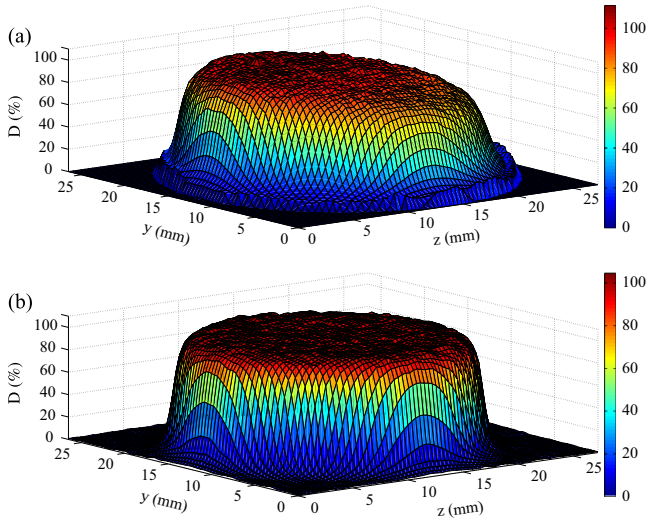

Fig. 6. (a) Measured 3D dose profile obtained by EBT3 gafchromic films analysis. (b) Calculated 3D dose profile by GEANT4 simulations.

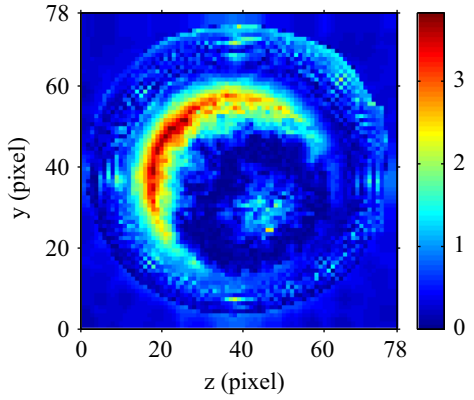

Fig. 7. Color map representing the γ dose distribution comparison technique. At 80% of the points a γ index less than 1 corresponds.

To confirm that the simulated and experimental PDD curves are comparable a validation test was performed. The metric test, that was explained in the previous section, was performed with simulated and experimental PDD curves obtained in the vacuum. The test showed a percentage error of 2%.

In the two-dimensional dose distribution along the vertical axis *y*, it can be noted that the right side with respect to the symmetry axis overlaps with the simulated one well enough, while the left side profile has a different trend. However, in the two-dimensional dose distribution along the horizontal axis *z*, the experimental left side profile matches the simulated profile (Fig. 5).

3D dose profiles were also analyzed (Fig. 6). To compare simulated and experimental profiles, the test that calculates γ index [23], developed in Matlab software was run. The tolerances considered in terms of distance-to-agreement between the two curves and in dose-difference were respectively 3 mm and 3% [24]. The test was exceeded in the points where the gamma value was less than 1.

The percentage of points to which a γ index less than 1 corresponds is about 80% (Fig. 7).

4. Conclusions and discussions

In this work we have presented a new Monte Carlo tool, based on the GEANT4 toolkit, aimed to design, optimize and characterize a laser-driven acceleration system specifically devoted to biological/medical applications. The *laser_IOERT* application allows to obtain a dosimetric characterization of table top laser-driven accelerators for radiobiology and preclinical experiments.

The metric test to compare simulated and experimental PDD curves in vacuum has shown a maximum percentage error of 2%. The error obtained is smaller than the dose-difference criteria imposed in the computation of the gamma index. Therefore we considered that the two curves are comparable, that is they come from the same function.

From the two-dimensional dose distributions we determined that the dose profiles obtained from experimental measurements do not agree completely with the simulated ones. This suggests that the electron beam is not generated in a totally uniform way.

A hypothesis could be that the point of interaction between the laser and the gas is not exactly centered on the axis of symmetry of the system. Indeed, the electron beam can have a pointing instability because there is an intrinsic component of the electron beam that can be slightly asymmetric [25]. This issue is being studied by other GEANT4 Monte Carlo simulations.

The result of the test range applied to 3D dose profiles can be considered positive because, as we can see from the color map, the gamma curve is less than 1 in a wide area . This test gives us a confirmation of the validation of the GEANT4 application. Moreover, in the color map also the area in which the test is not positive is visible, that is it confirms the zone of non-uniformity of the generated electron beam.

The validated Geant4 application can be used to convey the appropriate data about the experimental set-up and to study dose distributions to be delivered for future radiobiological measurements and future preclinical experiments.

Acknowledgments

This work was supported by FIRB/MERIT (RBNE089KHH). The activity of the INO-CNR Pisa group was partially supported from the Italian Ministry of Health through the Project no. GR-2009-1608935 (Study of Radiobiological and Radiotherapic Effects of a Novel Laser-Driven Electron Accelerator, D.I. AgeNaS), from the CNR funded Italian research Network ELI-Italy (Attoseconds) and from the PRIN project (Contract no. PRIN2012AY5LEL). The Pisa authors also acknowledge contribution from the MIUR-FIRB project SPARX (Sorgente Pulsata Auto-Amplificata di Radiazione X) and the INFN Plasma-med collaboration.

References

[1] V. Malka, J. Faure, Y. Glinec, C. Rechatin, Journal of Physics: Conference Series 112 (4) (2008) 042029, URL ⟨http://stacks.iop.org/1742-6596/112/i=4/a=042029⟩.

[2] M. Martin, Journal of the National Cancer Institute 101 (7) (2009) 450. http://dx.doi.org/10.1093/jnci/djp071, URL ⟨http://jnci.oxfordjournals.org/content/101/7/450.short⟩.

[3] E. Esarey, C.B. Schroeder, W.P. Leemans, Reviews of Modern Physics 81 (2009) 1229. http://dx.doi.org/10.1103/RevModPhys.81.1229, URL http://dx.doi.org/link.aps.org/doi/10.1103/RevModPhys.81.1229.

[4] J. van Tilborg, C.B. Schroeder, C.V. Filip, C. Tóth, C.G.R. Geddes, G. Fubiani, R. Huber, R.A. Kaindl, E. Esarey, W.P. Leemans, Physical Review Letters 96 (2006) 014801. http://dx.doi.org/10.1103/PhysRevLett.96.014801, URL http://dx.doi.org/link.aps.org/doi/10.1103/PhysRevLett.96.014801.

[5] L. Labate, M.G. Andreassi, F. Baffigi, G. Basta, R. Bizzarri, A. Borghini, G.C. Candiano, C. Casarino, M. Cresci, F. Di Martino, L. Fulgentini, F. Ghetti, M.C. Gilardi, A. Giulietti, P. Kster, F. Lenci, T. Levato, Y. Oishi, G. Russo, A. Sgarbossa, C. Traino, L.A. Gizzi, Small-scale laser based electron accelerators for biology and medicine: a comparative study of the biological effectiveness *Proc. SPIE* 8779, Laser Acceleration of Electrons, Protons, and Ions II; and Medical Applications of Laser-Generated Beams of Particles II; and Harnessing Relativistic Plasma Waves III, 87790O (May 7, 2013), http://dx.doi.org/10.1117/12.2019689.

[6] J. Allison, K. Amako, J. Apostolakis, H. Araujo, P. Dubois, M. Asai, G. Barrand, R. Capra, S. Chauvie, R. Chytracek, G. Cirrone, G. Cooperman, G. Cosmo,

G. Cuttone, G. Daquino, M. Donszelmann, M. Dressel, G. Folger, F. Foppiano, J. Generowicz, V. Grichine, S. Guatelli, P. Gumplinger, A. Heikkinen, I. Hrivnacova, A. Howard, S. Incerti, V. Ivanchenko, T. Johnson, F. Jones, T. Koi, R. Kokoulin, M. Kossov, H. Kurashige, V. Lara, S. Larsson, F. Lei, O. Link, F. Longo, M. Maire, A. Mantero, B. Mascialino, I. McLaren, P. Lorenzo, K. Minamimoto, K. Murakami, P. Nieminen, L. Pandola, S. Parlati, L. Peralta, J. Perl, A. Pfeiffer, M. Pia, A. Ribon, P. Rodrigues, G. Russo, S. Sadilov, G. Santin, T. Sasaki, D. Smith, N. Starkov, S. Tanaka, E. Tcherniaev, B. Tome, A. Trindade, P. Truscott, L. Urban, M. Verderi, A. Walkden, J. Wellisch, D. Williams, D. Wright, H. Yoshida, IEEE Transactions on Nuclear Science NS-53 (1) (2006) 270. http://dx.doi.org/10.1109/TNS.2006.869826.

[7] C. Fiandra, R. Ragona, U. Ricardi, S. Anglesio, F.R. Giglioli, Medical Physics 35 (12) (2008) 5463. http://dx.doi.org/10.1118/1.3005975, URL http://scitation.aip.org/content/aapm/journal/medphys/35/12/10.1118/1.3005975.

[8] G.C. Bussolino, A. Faenov, A. Giulietti, D. Giulietti, P. Koester, L. Labate, T. Levato, T. Pikuz, L.A. Gizzi, Journal of Physics D: Applied Physics 46 (24) (2013) 245501, URL ⟨http://stacks.iop.org/0022-3727/46/i=24/a=245501⟩.

[9] G. Russo, C. Casarino, G. Arnetta, G. Candiano, A. Stefano, F. Alongi, G. Borasi, C. Messa, M. Gilardi, Dose distribution changes with shielding disc misalignments and wrong orientations in breast IOERT: a Monte Carlo GEANT4 and experimental study, Journal of Applied Clinical Medical Physics 13(5), 2012. URL ⟨http://www.jacmp.org/index.php/jacmp/article/view/3817⟩.

[10] Geant4 Collaboration, Physic Reference Manual of Geant4.9.5. URL ⟨http://geant4.web.cern.ch/geant4/⟩.

[11] J. Sempau, J. Fernndez-Varea, E. Acosta, F. Salvat, Nuclear Instruments and Methods in Physics Research Section B: Beam Interactions with Materials and Atoms 207 (2) (2003) 107. http://dx.doi.org/10.1016/S0168-583X(03)00453-1, URL ⟨http://www.sciencedirect.com/science/article/pii/S0168583X03004531⟩.

[12] G. Russo, C. Casarino, G.C. Candiano, L. Labate, F. Baffigi, G. Bussolino, L. Fulgentini, A. Giulietti, P. Koester, T. Levato, L. A. Gizzi, G. Borasi, C. Messa, M.C. Gilardi, A preliminary dosimetric characterization of a small-scale laser based electron accelerator: first steps towards a possible alternative to RF medical LINACs, 2013, URL ⟨http://www.aifm2013.org/topic/1radioterapia2.pdf⟩.

[13] J.M. Dawson, Reviews of Modern Physics 55 (1983) 403. http://dx.doi.org/10.1103/RevModPhys.55.403, URL http://dx.doi.org/link.aps.org/doi/10.1103/RevModPhys.55.

[14] V.C. Borca, M. Pasquino, G. Russo, P. Grosso, D. Cante, P. Sciacero, G. Girelli, M.R. L. Porta, S. Tofani, Journal of Applied Clinical Medical Physics 14 (2), 2013, URL ⟨http://www.jacmp.org/index.php/jacmp/article/view/4111⟩.

[15] SIT S.p.A. URL ⟨http://soiort.com/⟩.

[16] L. Menegotti, A. Delana, A. Martignano, Medical Physics 35 (7) (2008) 3078. http://dx.doi.org/10.1118/1.2936334, URL ⟨http://scitation.aip.org/content/aapm/journal/medphys/35/7/10.1118/1.2936334⟩.

[17] F.-C. Su, Y. Liu, S. Stathakis, C. Shi, C. Esquivel, N. Papanikolaou, Applied Radiation and Isotopes 65 (10) (2007) 1187. http://dx.doi.org/10.1016/j.apradiso.2007.05.005, URL ⟨http://www.sciencedirect.com/science/article/pii/S0969804307001601⟩.

[18] PTW URL ⟨http://www.ptw.de⟩.

[19] G.A.P. Cirrone, S. Donadio, S. Guatelli, A. Mantero, B. Mascialino, S. Parlati, M. Pia, A. Pfeiffer, A. Ribon, P. Viarengo, IEEE Transactions on Nuclear Science NS-51 (5) (2004) 2056. http://dx.doi.org/10.1109/TNS.2004.836124.

[20] L. Piegl, W. Tiller, The NURBS Book, Monographs in Visual Communication, U.S. Government Printing Office, 1997. URL ⟨http://books.google.it/books?id=7dqY5dyAwWkC⟩.

[21] International Atomic Energy Agency, Absorbed Dose Determination in External Beam Radiotherapy: An International Code of Practice for Dosimetry Based on Standards of Absorbed Dose to Water, 2000.

[22] F. Schneider, M. Polednik, D. Wolff, V. Steil, A. Delana, F. Wenz, L. Menegotti, Zeitschrift fr Medizinische Physik 19 (1) (2009) 29. http://dx.doi.org/10.1016/j.zemedi.2008.09.001, URL ⟨http://www.sciencedirect.com/science/article/pii/S0939388908001025⟩.

[23] T. Ju, T. Simpson, J.O. Deasy, D.A. Low, Medical Physics 35 (3) (2008) 879. http://dx.doi.org/10.1118/1.2836952.

[24] D.A. Low, W.B. Harms, S. Mutic, J.A. Purdy, Medical Physics 25 (5) (1998) 656. http://dx.doi.org/10.1118/1.598248, URL ⟨http://scitation.aip.org/content/aapm/journal/medphys/25/5/10.1118/1.598248⟩.

[25] G. Grittani, M. Anania, G. Gatti, D. Giulietti, M. Kando, M. Krus, L. Labate, T. Levato, P. Londrillo, F. Rossi, L. Gizzi, Nuclear Instruments and Methods in Physics Research Section A: Accelerators, Spectrometers, Detectors and Associated Equipment 740 (0) (2014) 257; in: Proceedings of the First European Advanced Accelerator Concepts Workshop 2013. http://dx.doi.org/10.1016/j.nima.2013.10.082. URL ⟨http://www.sciencedirect.com/science/article/pii/S0168900213014897⟩.